Computational Modeling of Oxygen Isotope Effects on Metal-Mediated O_2 Activation at Varying Temperatures†

Valeriy V. Smirnov,‡ Michael P. Lanci,⊥ and Justine P. Roth*

Department of Chemistry, Johns Hopkins University, 3400 North Charles Street, Baltimore, Maryland 21218

Received: September 2, 2008; Revised Manuscript Received: October 17, 2008

Oxygen equilibrium isotope effects (^{18}O EIEs) upon the formation of metal superoxide and peroxide structures from natural abundance O_2 are reported. The ^{18}O EIEs determined over a range of temperatures are compared to those calculated on the basis of vibrational frequencies. Considering all vibrational modes in a "full frequency model" is found to reproduce the empirical results better than "cut-off" models which consider only the most isotopically sensitive modes. Theoretically, the full frequency model predicts that ^{18}O EIEs arise from competing enthalpic and entropic influences resulting in nonlinear variations with temperature. Experimental evidence is provided for an increase in the magnitude of the EIE, in some instances implicating a change from inverse to normal values, as the temperature is raised. This finding is not easily reconciled with the common intuition that ^{18}O EIEs arise from a reduction of the O−O force constant and attendant changes in zero point energy level splitting. Instead a dominant entropic effect, as described here, is expected to characterize isotope effects upon reversible binding of small molecules to metal centers in enzymes and inorganic compounds.

Introduction

Stable isotope fractionation[1,2] has become a universal tool for investigating chemical and biological reactivity in defined as well as complex environments.[3−6] Methods have been developed for the study of carbon-13, nitrogen-15, and oxygen-18 isotope effects on reactions of organic compounds in addition to a variety of small molecules (e.g., O_2, N_2, and CO_2).[4] The oxygen-18 fractionation technique, in particular, has been applied to a range of important problems from the atmospheric production of ozone[7] to the effects of pollutants on human respiration.[8] Yet the ability to extract detailed structural and mechanistic information from the isotope effect in these studies remains a challenge.[9]

Our recent efforts have concentrated on the use of oxygen isotope effects to probe the oxidative reactivity of inorganic compounds and metalloenzymes, specifically that involving molecular oxygen (O_2).[9a,b] To advance established approaches,[9c] we have developed methods for analyzing related isotope effects on reactions of superoxide ($O_2^{\bullet-}$)[10,11] and hydrogen peroxide (H_2O_2).[12] An important goal for this research is to use oxygen equilibrium isotope effects (^{18}O EIEs) to relate the reactions of O_2, $O_2^{\bullet-}$, and H_2O_2 to one another and as well as to illuminate the constituent kinetic isotope effects (^{18}O KIEs) upon the formation of oxygen-derived intermediates.

The requirement of characterizing structures of activated oxygen intermediates in terms of molecular vibrations makes density functional theory (DFT) a vital complement to these studies. Though DFT has been used extensively to describe barriers to small molecule activations in biological[13,14] and chemical settings,[15] calibration of the methodology to predict isotape effects is often difficult. Here we propose that the comparison of experimental to computed oxygen isotope effects provides an effective way to evaluate ground and possibly transition state structures.

^{18}O KIEs and ^{18}O EIEs have been determined for a number of O_2 activation reactions and analyzed within the context of experimental stretching frequencies.[10,16,17] In the vast majority of cases, ^{18}O KIEs upon reactions of O_2 have been interpreted by using the ^{18}O EIE, defined simply according to eq 1, as an upper limit.[9c] The relationship ^{18}O KIE < ^{18}O EIE can be derived from Transition State Theory and the definition in eq 2, which neglects nuclear tunneling and isotopic differences in transmission coefficient. When the isotope effect upon the reaction coordinate frequency, the mode that converts a translation into a vibration at the transition state, is negligible ($^{16,16}\nu_{RC}/^{16,18}\nu_{RC} \approx 1$), the ^{18}O KIE is equivalent to the pseudoequilibrium constant for converting the reactant to the transition state ($^{16,16}K_{TS}/^{16,18}K_{TS}$). Since the transition state is associated with a structure having vibrational frequencies intermediate of the reactant and product, the relationship $^{16,16}K_{TS}/^{16,18}K_{TS} <$ ^{18}O EIE is expected to hold.[17]

$$^{18}\text{O EIE} = {}^{16,16}K_{eq}/{}^{16,18}K_{eq} \quad (1)$$

$$^{18}\text{O KIE} = \left({}^{16,16}\nu_{RC}/{}^{16,18}\nu_{RC}\right) \times \left({}^{16,16}K_{TS}/{}^{16,18}K_{TS}\right) \quad (2)$$

While the literature is rife with discussions of how ν_{RC} may contribute significantly to heavy atom KIEs,[3b] few studies have computationally examined the reaction coordinate for binding of small molecules to heavier metal fragments.[18] It can be difficult to define a saddle point structure and consequently estimate ν_{RC} for such reactions of O_2, where a new metal−O bond is formed at the same time the O−O is weakened. Interestingly, experiments have revealed that the ^{18}O KIEs are highly variable, yet in all cases are smaller than the ^{18}O EIEs which are similar for the related reversible O_2 binding reactions.[17] These results have been taken as support for the assumption that the ^{18}O KIE < ^{18}O EIE and that the $^{16,16}\nu_{RC}/^{16,18}\nu_{RC}$ contribution can be neglected.[17] To our knowledge, an alternative possibility where $^{16,16}\nu_{RC}/^{16,18}\nu_{RC}$ is a primary determinant of

† Part of the "Max Wolfsberg Festschrift".

* Corresponding author. E-mail: jproth@jhu.edu.

‡ Present address: Department of Chemistry, University of Montana, Missoula, Montana 59812.

⊥ Present address: Department of Chemistry, University of Washington, Seattle, Washington 98195.

10.1021/jp807796c CCC: $40.75
Published on Web 01/02/2009

CHART 1: Transition Metal Superoxide and Peroxide Compounds with Abbreviations Used in This Study

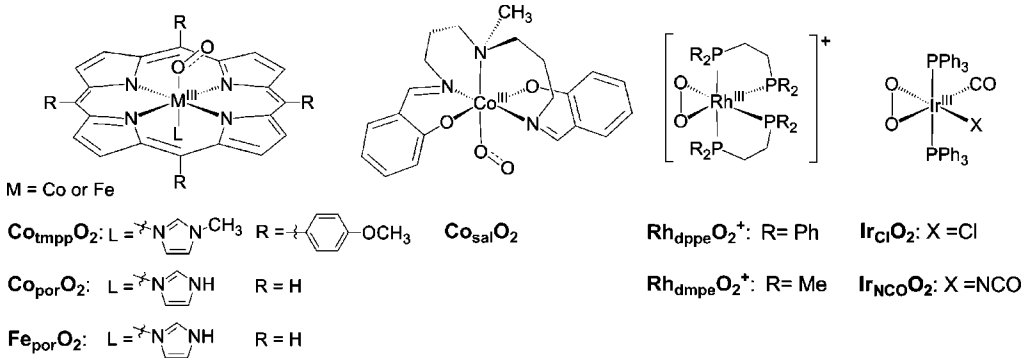

the ^{18}O KIE, which varies within the limits set by the ^{18}O EIE, has not been considered.

As a first step toward refining computational methods for studies of isotope effects upon O_2 activation, the following report describes ^{18}O EIEs determined by using an established natural abundance/competitive isotope fractionation method.[9] Measurements were performed on structurally defined O_2-carrier molecules formally described as cobalt(III) end-on superoxide (η^1-O_2^{-I}) and rhodium(III) side-on peroxide (η^2-O_2^{-II}) adducts (Chart 1). The ^{18}O EIEs were determined by using pre-equilibrated solutions by analyzing the $^{18}O/^{16}O$ composition of the O_2 released from the inorganic compound. The experimental ^{18}O EIEs are compared to those calculated by using two different types of models, a "full-frequency" model that considers all vibrations associated with the isotopic molecules and a "cutoff" model that employs only three isotope-dependent vibrations for the metal and O_2. The cutoff approach was originally popularized by Stern and Wolfsberg[19] for large molecules before high-level electronic structure calculations were readily available. Although Stern and Wolfsberg may not have recommended the analogous approach be extended to reactions of small moelcules, such methods have been used extensively to interpret experimental studies of ^{18}O EIEs on reactions of O_2.[9a,10,16,17]

The present studies evaluate the abilities of full-frequency and cutoff models to reproduce variations in ^{18}O EIEs over large ranges in temperature. Due to the bimolecular nature of the O_2 binding reactions under consideration, compensating influences of both enthalpy and entropy are expected to determine the reaction spontaneity as well as the isotope effects. Upon coordinating O_2 to a redox metal center, low-frequency metal−oxygen vibrations are created at the expense of the mass-dependent translations and rotations in free O_2. The conversion of these mass-dependent degrees of freedom in O_2 to new, low-frequency vibrations in the end-on superoxide and side-on peroxide structures results in ^{18}O EIEs that exhibit distinctive variations with temperature. The reliable prediction of these trends requires the accurate assessment of the net isotope shifts of all vibrations within O_2 and the oxygenated product.

Experimental Section

1. Methods and Materials. Manipulations of air- and moisture-sensitive materials were performed by using Schlenk techniques or a N_2-filled glovebox (MBraun). Reagents were obtained from Aldrich in the highest purity available and purified according to standard protocols.[20] "Anhydrous" *N*,*N*-dimethylformamide (DMF) obtained from Burdick & Jackson was stored in the glovebox freezer to prevent decomposition and sparged with N_2 to remove volatile impurities prior to use. Chlorobenzene (ClBz) (Fisher Scientific) was twice vacuum transferred after drying over P_2O_5 for >12 h. MeTHF (Aldrich) was dried over Na^0/benzophenone. Compressed air (zero grade) and oxygen (extra dry grade) were obtained from Airgas and further purified by passing through a column of anhydrous calcium sulfate (Drierite). Transition metal compounds were prepared following published procedures.[21] As described in earlier work,[22] purity was assessed by elemental analysis, multinuclear NMR spectroscopy, and the analysis of molar extinction coefficients in the UV−visible region. Electronic absorbance spectra were recorded on an Agilent 8453 UV−visible spectrophotometer equipped with a peltier (89090-A) temperature controller. NMR spectroscopy was performed with a Bruker Avance 300 MHz spectrometer with a temperature calibrated probe.

2. Assessing the Reversibility of O_2 Binding. Equilibrium constants for the reversible coordination of O_2 were evaluated by using manometry and spectroscopy at varying temperatures. Measurements of O_2 pressure and isotope composition were performed simultaneously with a home-built vacuum apparatus equipped with a reaction chamber, combustion furnace (for converting O_2 to CO_2), and calibrated capacitance manometer.[22] Reaction solutions were saturated with 1 atm of dry air or oxygen at the desired temperature. The pressure of O_2 obtained from solution aliquots with and without the transition metal compound present was determined and related to the concentrations of unbound and metal-bound O_2 present at equilibrium. The results agreed with those determined by spectroscopy under the analogous conditions.

3. Equilibration of Reaction Mixtures. Equilibrium is rapidly established for **Co$_{sal}$O$_2$** and **Co$_{tmpp}$O$_2$** consistent with previous reports.[23,24] The equilibration of **Rh$_{dppe}$O$_2^+$** is much slower due to the higher barriers to O_2 coordination and release. For this reaction, O_2 binding rate constants were determined at temperatures between 283 and 313 K by monitoring the optical band at $\lambda_{max} = 404$ nm associated with the rhodium(I) starting material, **Rh$_{dppe}^+$**.[25] Experiments were conducted under a pseudo-first-order excess of O_2. The data were analyzed according to eq 3, where $[A]_{eq}$ and $[A]_0$ are the equilibrium and initial concentrations of **Rh$_{dppe}^+$**, respectively, [A] is the concentration of **Rh$_{dppe}^+$** at time (t), and $k_{on}' = k_{on} \times [O_2]$.[26]

$$\left(1 - \frac{[A]_{eq}}{[A]_0}\right) \ln \frac{(1 - [A]_{eq}/[A]_0)}{(1 - [A]_{eq}/[A])} = k_{on}' t \qquad (3)$$

Plotting the left side of eq 3 versus t gives a straight line with a slope of k_{on}', when $[A]_{eq}$ is the [**Rh$_{dppe}^+$**] at equilibrium. The equilibrium constant is readily calculated from eq 4. The rate constant for the reverse reaction (k_{off}) can subsequently be estimated from $K_{eq} = k_{on}/k_{off}$.

$$K_{eq}=([A]_0-[A]_{eq})/([A]_{eq}[O_2]) \quad (4)$$

Analysis of the data between 283 and 313 K yielded thermodynamic parameters as well as the activation parameters corresponding to the formation of $\mathbf{Rh_{dppe}O_2^+}$. The Eyring equation[26] was used to extrapolate to rate constants outside the experimental range, to temperatures as low as 213 K, assuming no curvature. The k_{on} and k_{off} were used in kinetics simulations, with the program KinSim,[27] to approximate the time required for $\mathbf{Rh_{dppe}O_2^+}$ to reach equilibrium at each temperature.

The equilibration time period was estimated by plotting $[\mathbf{Rh_{dppe}}^+]/[\mathbf{Rh_{dppe}}^+]_0$ versus time according to eq 5, and then finding the point at which the slope stopped changing. In eq 5, [A] is the concentration of the absorbing species, $\mathbf{Rh_{dppe}}^+$, at time t. $[A]_0$ is the initial $\mathbf{Rh_{dppe}}^+$concentration, $k_{on}' = k_{on} \times [O_2]$ and $K'_{eq} = k_{on}'/k_{off}$. The $[A]/[A_0]$ approaches a constant value as the system nears the equilibrium. The equilibration time estimated in this way was confirmed independently by performing isotope fractionation measurements on fully equilibrated samples and comparing the results to those of purposely nonequilibrated samples.

$$\frac{[A]}{[A]_0}=\frac{1+K'_{eq}\exp[-(k_{on}'+k_{off})\times t]}{1+K'_{eq}} \quad (5)$$

4. Measurement of ^{18}O EIEs. Detailed descriptions of the apparatus and methodology used to determine ^{18}O EIEs have been published elsewhere.[22,28] Samples of O_2 were isolated from solutions that contained no additional reactant or those which contained a transition metal$-O_2$ adduct in equilibrium with its reduced form. The isolated O_2 was purified from other condensable gases and quantitatively combusted to CO_2 to facilitate handling. The CO_2 samples were placed in dry glass tubes and flame-sealed, later to be analyzed with a dual-inlet isotope ratio mass spectrometer at the University of Waterloo Environmental Isotope Laboratory (uwEILAB), Waterloo, Ontario, Canada. Ratios of ^{18}O to ^{16}O were reported versus standard mean ocean water (SMOW) with precisions of ± 0.0002.

The determination of ^{18}O EIEs sometimes required equilibration over extended time periods. Samples were incubated by using a recirculating bath (VWR Model 1190S) to control temperatures between 243 and 313 K. A different type of cooling apparatus was used below 243 K. For reactions that equilibrated in <8 h, solutions were prepared in a modified reaction chamber[29] equipped with a jacketed Dewar. Temperature was controlled by using slurries of pentane (153 K), THF (164 K), DMF (213 K), and acetonitrile (228 K) mixed with liquid nitrogen or 2-propanol (195 K) mixed with dry ice. For reactions that required >8 h to equilibrate, premixed solutions were placed in Schlenk tubes and stirred continuously in an immersion chiller (Cryocool CC-100II, NESLAB Instruments). These solutions were transferred via a stainless steel cannula into the precooled reaction chamber.

Experiments were conducted under an atmosphere of O_2 or air, at natural abundance, in the reaction chamber attached to the vacuum apparatus. Due to solubility and stability constraints, measurements employed the polar solvent DMF ($\epsilon = 36.7$ at 293 K) and the relatively nonpolar solvents MeTHF ($\epsilon = 5.62$ at 293 K) and ClBz ($\epsilon = 7.58$ at 293 K). The activation parameters for $\mathbf{Co_{sal}O_2}$ and $\mathbf{Co_{tmpp}O_2}$ indicate that reactions should reach equilibrium within minutes at the lowest temperatures examined.[23,24] Resaturating the depleted solution with air takes several minutes at 153 K even with vigorous bubbling and stirring. Thus, a period of 45 min was allowed between samples for the determination of ^{18}O EIEs. Allowing for longer times (>4 h) did not significantly affect the results.

CHART 2: Isotope Exchange for End-On Superoxide (a) and Side-On Peroxide (b) Structures[a]

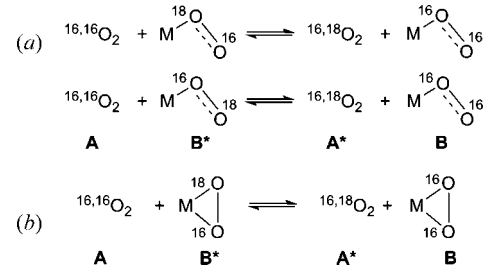

[a] **A** and **B** correspond to O_2 and the oxygenated product, respectively. The asterisk designates the site of ^{18}O.

The ^{18}O EIEs were calculated from the pressure and isotope composition of the CO_2, which are identical to that of the O_2 isolated from solution. According to eq 6, R_t is the $^{18}O/^{16}O$ in the total O_2 isolated from solutions containing the metal$-O_2$ adduct, R_u is the $^{18}O/^{16}O$ in the O_2 isolated from solutions containing only the gas and no transition metal compound, and $1-f$ is the fraction of the metal-bound O_2 that was determined from the change in pressure upon adding the reduced transition metal compound to an O_2 or air-saturated solution and allowing for equilibrium to be attained. Only samples that showed a significant uptake of O_2 ($1-f$) > 0.1 were analyzed. The ^{18}O EIE at each temperature was determined as the average of multiple independent measurements and reported with errors of ± 1 standard deviation about the mean.

$$^{18}\text{O EIE}=\frac{1-f}{R_t/R_u-f} \quad (6)$$

5. Computational Analysis of Vibrational Frequencies. Molecular geometries were fully optimized at the density functional level of theory (DFT) by using the modified exchange and correlation functionals of Perdew and co-workers *m*PWPW91[30] as implemented in Gaussian03.[31] The atomic orbital basis functions used in the calculations are given in parentheses: Co, Fe, and Cl (the compact relativistic effective core potential basis CEP-31G),[32] N and O (6-311G*), P (6-311G**), C(6-31G), and H (STO-3G).[33,34a] For Rh, the LANL2DZ basis set with effective core potentials was employed. The stability of the final wave function solution was confirmed for each optimized structure. SOMOs and HOMOs were visualized and associated with either the metal or O_2. No imaginary modes were indicated for any of the optimized geometries.

The *m*PWPW91 functional along with the 6-311G* basis on oxygen was chosen for its ability to reproduce the absolute stretching frequency of O_2 and the vibrational frequency shift upon isotope substitution.[34] This DFT method had previously been shown to accurately reproduce the experimental isotope effect for a related reaction. To test the influence of solvent polarity upon ^{18}O EIE,[35] geometries were optimized within a polarized continuum model (PCM) which included the solvation effects of DMF, ClBz, and THF. Solvent polarity is expected to enhance charge transfer to oxygen within the metal$-O_2$ adduct, thereby increasing the O$-$O bond length and decreasing the stretching frequency.

6. Calculations of ^{18}O EIEs. ^{18}O EIEs were calculated by using the formalism of Bigeleisen and Goeppert$-$Mayer,[36] in which the isotope effect is equal to the equilibrium constant for an isotope exchange reaction. The chemical equation for such a reaction is obtained by subtracting the individual equilibria associated with the heavy and light isotopologues; this is equivalent to dividing the individual equilibrium con-

stants, i.e., ^{18}O EIE = $K(^{16}O^{16}O)/K(^{16}O^{18}O)$. The isotope exchange reactions are shown in Chart 2 for the end-on (η^1) and side-on (η^2) binding of O_2. In the latter case, symmetry equates the positions of the oxygen nuclei.

The ^{18}O EIEs associated with the isotope exchange reactions can be defined in terms of three reduced partition functions (eq 7). These contributions include the isotopic differences in zero-point energy (ZPE), energy of the excited vibrational states (EXC), and the mass and moments of inertia (MMI) (eqs 8−11).[37] Two expressions are given for MMI, the first of which (eq 10) is a consequence of the Redlich−Teller Product Rule.[38] The second expression for MMI (eq 11) is derived from the rigid rotor approximation where M is the molecular mass and I represents the moment of inertia.

$$^{18}\text{O EIE} = \text{ZPE} \times \text{EXC} \times \text{MMI} \tag{7}$$

$$\text{ZPE} = \frac{\left[\prod_j^{3N-6} \frac{e^{(h\nu_j^{B*}/2kT)}}{e^{(h\nu_j^{B}/2kT)}}\right]}{\left[\prod_i^{3N-5} \frac{e^{(h\nu_j^{A*}/2kT)}}{e^{(h\nu_j^{A}/2kT)}}\right]} \tag{8}$$

$$\text{EXC} = \frac{\left[\prod_j^{3N-6} \frac{1-e^{(h\nu_j^{B*}/kT)}}{1-e^{(h\nu_j^{B}/kT)}}\right]}{\left[\prod_i^{3N-5} \frac{1-e^{-(h\nu_j^{A*}/kT)}}{1-e^{-(h\nu_j^{A}/kT)}}\right]} \tag{9}$$

$$\text{MMI} = \text{VP} = \frac{\prod_j^{3N-6} \left(\nu_j^{B}/\nu_j^{B*}\right)}{\prod_i^{3N-5} \left(\nu_j^{A}/\nu_j^{A*}\right)} \tag{10}$$

$$\text{MMI} = \frac{\left[\left(\frac{^{16,16}M}{^{16,18}M}\right)^{3/2} \times \prod_j^{n_{rot}} \left(\frac{^{16,16}I}{^{16,18}I}\right)^{1/2}\right]_{final}}{\left[\left(\frac{^{16,16}M}{^{16,18}M}\right)^{3/2} \times \prod_i^{n_{rot}} \left(\frac{^{16,16}I}{^{16,18}I}\right)^{1/2}\right]_{initial}} \tag{11}$$

Most discussions of ^{18}O EIEs for end-on (η^1) O_2 adducts have neglected the preference for heavy oxygen coordinating to the metal.[28,29] The assumption is generally made that equal fractions of M−^{18}O−^{16}O and M−^{16}O−^{18}O contribute to the isotope effect. In the appendix to this article we present an alternative analysis where the isotopic preference is considered explicitly through the contributions of the individual isotope effects. The ^{18}O EIE can be calculated as a weighted geometric mean[39a]of the M−^{18}O−^{16}O and M−^{16}O−^{18}O coordination modes relative to M−^{16}O−^{16}O (eq 12). The weighting term, α, representing the fraction of the metal−O_2 adduct with ^{16}O−^{18}O coordinated via the heavy isotope is calculated directly from the vibrational frequencies (eq 13).

$$^{18}\text{O EIE}_{WGM} = (^{18,16}\text{O EIE})^{\alpha} \times (^{16,18}\text{O EIE})^{(1-\alpha)} \tag{12}$$

$$\alpha = \frac{1}{1 + \frac{^{18,16}\text{O EIE}}{^{16,18}\text{O EIE}}} \tag{13}$$

For the end-on superoxide species in this study, where two bonding modes are possible, the ^{18}O EIE and constituent partition functions were calculated as the weighted geometric means per eqs 12 and 13. The preference of the heavy isotope for the metal, as manifested in the inverse $^{18,16}O$ EIE, is thus explicitly taken into account. It follows from eq 13 that α = 1/2 when $^{18,16}O$ EIE = $^{16,18}O$ EIE and there is no coordination preference. In this case, eq 12 can be replaced by the geometric average of $^{18,16}O$ EIE and $^{16,18}O$ EIE.[39b] The difference between the $^{18,16}O$ EIE and $^{16,18}O$ EIE is expected to decrease as the temperature rises and the populations of vibrationally excited states corresponding to the different coordination modes become equal. For the reactions examined in this work, the weighted geometric mean ^{18}O EIE is found to be indistinguishable from the arithmetic and harmonic means at $T > 80$ K.

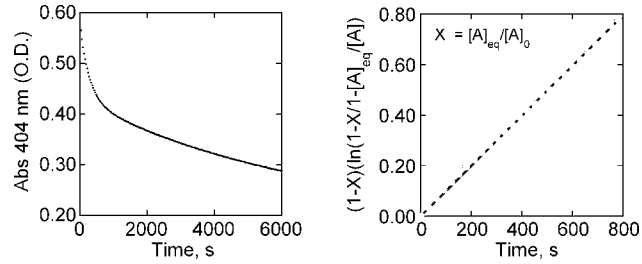

Figure 1. Left panel: Change in absorbance upon formation of $\mathbf{Rh_{dppe}O_2}^+$ at 293 K; $[\mathbf{Rh_{dppe}}^+]_0 = 1.2 \times 10^{-4}$ M, $[O_2] = 1.4 \times 10^{-3}$ M. Right panel: The first 800 s of data from the left panel fitted to eq 3. The results of the fit are $[\mathbf{Rh_{dppe}}^+]_{eq} = 0.81 \times 10^{-4}$ M, $K_{eq} = 344$ M^{-1}, $k_{on} = 0.7143$ M^{-1} s^{-1}, and $k_{off} = 0.0021$ s^{-1}.

Results

We have probed the variation in O_2 binding ^{18}O EIEs as a function of temperature and tested whether the experimental trends can be modeled using DFT calculations in light of the established theory.[36,37] Due to the small size of the ^{18}O KIE, the time scale for isotopic equilibrium is assumed to be the same as that of the corresponding chemical equilibrium. Some measurements were intentionally performed on nonequilibrated samples to determine the impact upon isotope fractionation and the apparent ^{18}O EIE.

In earlier works from different laboratories, inorganic compounds and metalloproteins were shown to satisfy the requirements of reversibility and equilibration at a single temperature. The following ^{18}O EIEs were reported[22,28,40] for the superoxide and peroxide structures in Chart 1: 1.0039 ± 0.0002 (oxyHb in water at 298 K), 1.0054 ± 0.0006 (oxyMb in water at 298 K), 1.0041 ± 0.0011 ($\mathbf{Co_{sal}O_2}$ in DMF at 259 K), 1.0053 ± 0.0017 ($\mathbf{Co_{sal}O_2}$ in ClBz at 245 K), 1.0066 ± 0.0013 ($\mathbf{Co_{tmpp}O_2}$ in ClBz at 245 K), 1.0199 ± 0.0017 ($\mathbf{Rh_{dppe}O_2}^+$ in DMF at 295 K), 1.0226 ± 0.0013 ($\mathbf{Ir_{NCO}O_2}$ in DMF at 295 K), and 1.0305 ± 0.0023 ($\mathbf{Ir_{Cl}O_2}$ in DMF at 295 K). In this study, we have expanded the temperature range to probe the variations in the ^{18}O EIE for the inorganic molecules. Only the cobalt and rhodium compounds were investigated due to practical considerations related to stability and equilibration time.

1. Challenges Associated with Slowly Equilibrating Reactions. The estimation of the activation parameters for $\mathbf{Rh_{dppe}O_2}^+$ formation and its dissociation to $\mathbf{Rh_{dppe}}^+$ and O_2 is described in the Experimental Section. In Figure 1, the left panel demonstrates disappearance of $\mathbf{Rh_{dppe}}^+$ absorbance at 404 nm in ClBz and the right panel shows the fit of the data collected during the first 800 s at 293 K. The $K_{eq} = 344$ M^{-1} derived from the spectrophotometric results compares favorably to the $K_{eq} = 395 \pm 52$ M^{-1} estimated by $^{31}P\{^1H\}$ NMR experiments at the same temperature. The level of internal agreement instills confidence that under the conditions used to determine ^{18}O EIE, the samples were fully equilibrated. The kinetic and thermodynamic parameters used to estimate the equilibration times for ^{18}O EIE measurements are shown in Table 1.

TABLE 1: Thermodynamic and Kinetic Parameters Determined for $Rh_{dppe}O_2^+$ at a Standard State of 1 atm

solvent	$\triangle H$ (kcal/mol)	$\triangle S$ (eu)	$\triangle H^{\ddagger}_{on}$ (kcal/mol)	$\triangle S^{\ddagger}_{on}$ (eu)	$\triangle H^{\ddagger}_{off}$ (kcal/mol)	$\triangle S^{\ddagger}_{off}$ (eu)
DMF	-15.0 ± 1.0	-37 ± 3	8.0 ± 3.0	-33 ± 11	23.0 ± 3.2	4 ± 11
ClBz	-11.0 ± 2.0	-27 ± 5	8.3 ± 3.0	-31 ± 9	19.3 ± 3.6	-4 ± 10

As a test of the equilibration times required for $\mathbf{Rh_{dppe}O_2^+}$, isotope ratio measurements were performed on samples that were incubated at the reaction temperature for a fraction of the total time needed for equilibrium to be established. Fully equilibrated samples of $\mathbf{Rh_{dppe}O_2^+}$ exhibit ^{18}O EIEs of 1.0220 $\pm$ 0.0019 at 248 K and 1.0216 $\pm$ 0.0022 at 245 K. When the same samples were incubated for only ~20% of the required equilibration time, an inflated apparent ^{18}O EIE of 1.0301 $\pm$ 0.0021 was observed. Experiments were also performed at 233 K. In this case, similar apparent ^{18}O EIEs of 1.0281 $\pm$ 0.0016 and 1.0308 $\pm$ 0.0027 were measured after 6 and 144 h, respectively. These results suggest that in neither experiment was the sample fully equilibrated. The kinetic simulations used to determine reaction conditions were, therefore, disregarded and only data collected above 245 K included in the analysis.

The isotope fractionation upon formation of $\mathbf{Rh_{dppe}O_2^+}$ at temperatures below 245 K is expected to depend on time. In the absence of the reverse dissociation reaction, a significant deviation from the actual ^{18}O EIE is expected; whether the value will be lower or higher depends upon the relative magnitudes of the ^{18}O KIE and ^{18}O EIE. In most cases this relationship is not known. It has been assumed, however, that the contribution from the reaction coordination frequency should be negligible making the ^{18}O EIE an upper limit to the KIE.[17] The results obtained with $\mathbf{Rh_{dppe}O_2^+}$ at very low temperatures suggest a different situation. At early times, when there is very little product, the expression corresponding to the ^{18}O EIE (eq 6) will approximate the ^{18}O KIE for the reaction in the forward direction. On these grounds, the results obtained for nonequilibrated samples, which were higher than those for equilibrated samples, imply that the ^{18}O KIE for the formation of $\mathbf{Rh_{dppe}O_2^+}$ might be greater than the ^{18}O EIE at temperatures below 250 K.

2. ^{18}O EIE on O_2 Binding as a Function of Temperature. Experiments were conducted in solvents of varying polarity to test whether the dielectric constant could affect the vibrational stretching frequencies and, therefore, the ^{18}O EIEs. For O_2 activation, the polar solvent is believed to stabilize the O_2-adducts[15a,29,41] and could enhance charge transfer to the O−O fragment causing an increase in bond length and decrease in stretching frequency.

The temperature dependence of the ^{18}O EIE upon forming $\mathbf{Co_{sal}O_2}$ in solvents of differing polarity is shown in Figure 2. In DMF, the ^{18}O EIE increases from 1.0034 $\pm$ 0.0021 at 218 K to 1.0072 $\pm$ 0.0014 at 294 K. In MeTHF where the ^{18}O EIE increases from 1.0004 $\pm$ 0.0026 at 161 K to 1.0056 $\pm$ 0.0025 at 249 K. The comparable variations with temperature indicate that dielectric constant does not exert a major influence on the ^{18}O EIE for the formation of $\mathbf{Co_{sal}O_2}$. This observation is in contrast to the equilibrium constants for O_2 binding which are significantly enhanced by increasing solvent polarity.[22,23]

A similar temperature dependence of the ^{18}O EIE is observed for the other neutral end-on superoxide species, $\mathbf{Co_{tmpp}O_2}$. In MeTHF, the ^{18}O EIE actually appears inverse 0.9990 $\pm$ 0.0013 at 155 K and gradually increases to normal 1.0028 $\pm$ 0.0014 at 248 K (Figure 2). The inverse ^{18}O EIE is consistent with the enthalpic contribution (ZPE) to the ^{18}O EIE overriding the entropic contribution (EXC × MMI).[42] Isotope effects of similar magnitude are seen in biological systems where end-on superoxide structures are present with differing degrees of hydrogen bonding to the terminal oxygen. In cytochrome P450cam, myoglobin, and hemoglobin, the ^{18}O EIEs range from 1.0034 to 1.0054 at ambient temperature and physiological pH.[28,40]

In contrast $\mathbf{Rh_{dppe}O_2^+}$ exhibits ^{18}O EIEs in DMF and ClBz which appear to decrease slightly with increasing temperature. In DMF, the ^{18}O EIE is 1.0220 $\pm$ 0.0019 at 248 K and 1.0162 $\pm$ 0.0015 at 313 K. In ClBz, the ^{18}O EIE is 1.0274 $\pm$ 0.0016 at 246 K and 1.0142 $\pm$ 0.0028 at 295 K. As discussed above, the larger ^{18}O EIEs of ~1.03 observed below 245 K are likely to be overestimated due to insufficient equilibration times. Though as observed with the neutral $\mathbf{Co_{sal}O_2}$, the ^{18}O EIEs for the cationic $\mathbf{Rh_{dppe}O_2^+}$do not seem to be affected by solvent dielectric in spite of the equilibrium constants for O_2 binding (at 249 K) which vary from $K_{O2} = 1.2 \times 10^5$ M^{-1} in DMF to 5.7×10^3 M^{-1} in ClBz. Student's *t*-test indicates that the mean ^{18}O EIEs are not statistically different for the two solvents in the range of 262−295 K.

3. Computational Analysis of Vibrational Frequencies. Vibrational frequencies used to calculate ^{18}O EIEs were obtained by using a DFT method previously shown to reproduce the temperature-independent ^{18}O EIEs for a copper end-on superoxide compound.[29] The *m*PWPW91 functional and basis sets provided in the Experimental Section were used to determine the minimum energy geometries of the metal−O_2 adducts in Chart 1 as well as for the simplified three-atom models, Co(η^1-O_2) and Rh(η^2-O_2). Following geometry optimization, frequency calculations indicated no imaginary modes for any of the structures. All normal mode vibrations were used in the calculations of the ^{18}O EIEs, according to eqs 7−10, without scaling.

The "zero frequencies"[43] corresponding to the rotational and translational modes are obtained upon diagonalization of Cartesian force constant matrix and afforded by the DFT calculations. By definition, the six modes for a nonlinear polyatomic molecule and five modes for a linear molecule should all have frequencies equal to zero. Wolfsberg has suggested[43] that the absolute magnitude of these frequencies can be used to judge the reliability of the optimized geometry and computed molecular force field. In this study the absolute magnitudes of the "zero frequencies" were less than 11 cm^{-1} for the full structural models and less than 29 cm^{-1} for models

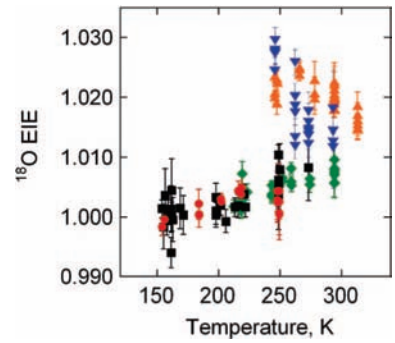

Figure 2. Natural abundance ^{18}O EIEs on the formation of $\mathbf{Co_{sal}O_2}$ in DMF (green diamonds) and MeTHF (black squares), $\mathbf{Co_{tmpp}O_2}$ in MeTHF (red circles), and $\mathbf{Rh_{dppe}O_2^+}$ in DMF (orange triangles) and ClBz (blue inverted triangles).

TABLE 2: Comparison of Calculated O−O Stretching Frequencies and Bond Lengths to Experimental Values

	ν_{O-O}(cm^{-1}) ($\nu^{16,18}$)		Bond Length d(O−O) (Å)	
structure/spin state[a]	exptl	calcd	exptl	calcd
O_2/triplet	1556.3 (43.8)[b]	1548.9 (43.7)	1.208[c]	1.221
Co(η^1-O_2)/doublet	1142−1154[d] (30−32)[e]	1154 (32)	1.26[f]	1.300
$Co_{sal}O_2$/doublet	1143−1146[g] (29−32)[e]	1227 (34)	1.06[h]	1.283
$Co_{tmpp}O_2$/doublet	1142−1154[d] (30−32)[e]	1246 (35)	1.26[f]	1.276
$Co_{por}O_2$/doublet	1142−1154[d] (30−32)[e]	1258 (35)	1.26[f]	1.286
$Fe_{por}O_2$/singlet	1139−1159[d] (30−33)[e]	1234 (35)	1.25[i]	1.277
$Fe_{por}O_2$/mixed[j]	1139−1159[d] (30−33)[e]	1232 (35)	1.25[i]	1.276
$Fe_{por}O_2$/triplet	1139−1159[d] (30−33)[e]	1256 (35)	1.25[l]	1.271
Rh(η^2-O_2)/singlet	888[k]	919 (26)	1.418[l]	1.429
$Rh_{dppe}O_2^+$/singlet	888[k]	921 (20)[m]	1.418[l]	1.408

[a] Abbreviations from Chart 1. Spin states are for energy minimized structures. [b] Reference 48. [c] Reference 49. [d] Reference 50. [e] $\nu_{16,18/18,16} = (\nu_{16,16} \times \nu_{18,18})^{1/2}$. [f] For oxycobaltomyoglobin, ref 45. [g] Reference 51. [h] Reference 44. [i] For oxymyoglobin, ref 52. [j] Broken-symmetry state that mixes singlet and triplet character, ref 53. [k] Reference 46. [l] Reference 47. [m] ν_{O-O} couples to the bending modes of the phenyl groups; overall $\Delta\nu_{16,18}$ is 25 cm^{-1}.

containing only three atoms. It is not uncommon for DFT calculations performed in default mode with Gaussian03 to give "zero frequencies" as high as 50 or 60 cm^{-1}; however, lower frequencies obtained with the more stringent optimization procedure can be close to 1 cm^{-1} indicating greater reliability of the computed isotope effects.

Calculated O−O bond lengths (d_{O-O}) and stretching frequencies (ν_{O-O}) are presented in Table 2 for comparison with the available experimental data. Though the calculations seem to systematically overestimate ν_{O-O}, agreement within 100 cm^{-1} is deemed reasonable in view of the variations which can be observed upon addition of a solvent correction.[29] The calculations reveal longer d_{O-O} and lower ν_{O-O} for the side-on structures than the end-on structures. In the case of **$Co_{sal}O_2$**, the calculated d_{O-O} differs significantly from the one determined by X-ray crystallography.[44] Yet the experimental bond length is questionable due to disorder of the dioxygen ligand.

The three-atom models, Co(η^1-O_2) and Rh(η^2-O_2), indicate d_{O-O} and ν_{O-O} comparable to the experimental data for **$Co_{sal}O_2$**, **$Co_{tmpp}O_2$**, and **$Rh_{dppe}O_2^+$** (Table 2). Best agreement is found when the Co(η^1-O_2) is optimized with a total charge = 0 and multiplicity = 2 and the Rh(η^2-O_2) is optimized with a total charge = −1 and multiplicity = 1. The use of extra electrons in these truncated models is apparently needed to compensate for the effects of the electron-releasing ligands that would normally be bound to the metal.

The optimized Co(η^1-O_2) structure exhibits d_{O-O} = 1.300 Å, d_{Co-O1} = 1.848 Å, and a nonbonded distance of d_{Co-O2} = 2.650 Å. The calculated O−O stretching frequency $^{16,16}\nu_{O-O}$ = 1153.8 cm^{-1} shifts to lower values upon isotope substitution ($\Delta\nu$ = 34.4 cm^{-1} for Co−^{16}O−^{18}O and 30.7 cm^{-1} for Co−^{18}O−^{16}O). The computational results compare favorably with the d_{O-O} = 1.26 Å and ν_{O-O} in the range from 1142 to 1154 cm^{-1} reported for other end-on cobalt superoxide structures such as the oxygenated form of cobalt-reconstituted myoglobin.[45]

The Rh(η^2-O_2) structure was minimized with constrained C_{2v} symmetry and diffuse functions were added to the oxygen basis set to accommodate the total negative charge on the molecule. The calculated d_{O-O} = 1.429 Å, d_{Rh-O} = 2.004 Å, and $^{16,16}\nu_{O-O}$ = 918.9 cm^{-1} ($\Delta\nu$ = 25.7 cm^{-1} for Rh^{16,18}O$_2$) are in reasonable agreement with the experimentally determined d_{O-O} = 1.418 Å and ν_{O-O} = 888 cm^{-1} for **$Rh_{dppe}O_2^+$**.[46,47] The three-atom models indicate O−O bond lengths and stretching frequencies which are in excellent agreement with the models of the actual structures (Table 2).

4. Analysis of the Temperature-Dependent ^{18}O EIEs. ^{18}O EIEs at varying temperatures were predicted within the formalism of Bigeleisen and Goeppert−Mayer by using full-frequency and computational three-atom cutoff models (Table 3).[36,37] Calculations were performed at 50−60 points between 0.15 and 1000 K. The quality was judged on the basis of agreement with the experimental results, inspection of the "zero frequencies", and deviations from the Redlich−Teller Product Rule. Wolfsberg has suggested these criteria for evaluating the reliability of computed isotopic partition functions.[43] As discussed above, the "zero frequencies" associated with the rotational and translational modes of the molecule should be zero. Deviations occur when the exact stationary point corresponding to the equilibrium geometry of the optimized structure is not found.[43] In the structural models described above, the "zero frequencies" range from 11 to 29 cm^{-1}, ^{18}O EIEs associated with the former giving superior agreement to the experimental results. In addition, deviation from the Redlich−Teller Product Rule was assessed by comparing MMI terms calculated by using two approaches. The MMI_{rot} derived from molecular masses and rotational constants (eq 12) should be the same as the MMI_{VP} derived from the ratio of vibrational frequencies (eq 11). For the full-frequency and computational three-atom cutoff models, the use of MMI_{rot} in place of MMI_{VP} would impart a deviation in the calculated ^{18}O EIE which is ±0.0005 and well within the experimental errors.

To further understand the physical origins of the ^{18}O EIEs, calculations were performed by using full-frequency models over an extended range of temperatures. The ^{18}O EIEs determined for the formation of **$Co_{sal}O_2$** and **$Rh_{dppe}O_2^+$** are typical of reactions where O_2 coordinates to a metal−ligand complex (Figure 3).[29] Though the overall trends are similar for metal−O_2 adducts, the positions of the EIE maxima for the η^1-superoxide structures occur at higher temperatures than the η^2-peroxide structures due to the contributions of the low-frequency vibrational modes.[54]

Within the full-frequency model, the inverse ZPE and EXC contributions are counterbalanced by a large normal MMI effect (1.144−1.155). Its size and relative invariance among the reactions examined is consistent with the loss of mass-dependent rotational and translational modes when O_2 binds to the much heavier metal fragment. Since new low-frequency modes are created, the product EXC × MMI is associated with the isotope effect on ΔS. The bonding changes are manifested in ZPE, which is consequently associated with the isotope effect on ΔH. Both contributions are predicted to depend on temperature over large ranges as shown in Figure 3.

In the two cases examined, the ^{18}O EIE begins inverse (<1), passes through a normal (>1) maximum, and then approaches

TABLE 3: ^{18}O EIEs and Reduced Partition Functions Based on Calculated Vibrational Frequencies

structure/mediumspin state	temp (K)[a]	mode	^{18}O EIE	ZPE	EXC	MMI	^{18}O EIE
Co(η^1-O_2)/vacuum (doublet)	116	$Co^{16}O-{}^{18}O$	1.0527	1.0300	0.9851	1.0374	1.0257
		$Co^{18}O-{}^{16}O$	1.0007	0.9518	0.9931	1.0587	
$Co_{sal}O_2$/vacuum (doublet)	391	$Co^{16}O-{}^{18}O$	1.0104	0.9781	0.9009	1.1466	1.0058
		$Co^{18}O-{}^{16}O$	1.0014	0.9484	0.9186	1.1495	
$Co_{sal}O_2$/THF (doublet)	370	$Co^{16}O-{}^{18}O$	1.0128	0.9782	0.9027	1.1469	1.0070
		$Co^{18}O-{}^{16}O$	1.0014	0.9448	0.9221	1.1494	
$Co_{sal}O_2$/DMF (doublet)	360	$Co^{16}O-{}^{18}O$	1.0137	0.9780	0.9041	1.1464	1.0076
		$Co^{18}O-{}^{16}O$	1.0016	0.9437	0.9237	1.1491	
$Co_{tmpp}O_2$/vacuum (doublet)	368	$Co^{16}O-{}^{18}O$	1.0102	0.9782	0.8942	1.1549	1.0062
		$Co^{18}O-{}^{16}O$	1.0023	0.9500	0.9130	1.1555	
$Co_{por}O_2$/vacuum (doublet)	369	$Co^{16}O-{}^{18}O$	1.0097	0.9779	0.9009	1.1461	1.0061
		$Co^{18}O-{}^{16}O$	1.0024	0.9513	0.9173	1.1487	
$Co_{por}O_2$/THF (doublet)	322	$Co^{16}O-{}^{18}O$	1.0141	0.9778	0.9067	1.1438	1.0089
		$Co^{18}O-{}^{16}O$	1.0037	0.9464	0.9242	1.1475	
$Fe_{por}O_2$/vacuum (singlet)	617	$Fe^{16}O-{}^{18}O$	1.0059	0.9827	0.8938	1.1453	1.0019
		$Fe^{18}O-{}^{16}O$	0.9978	0.9545	0.9100	1.1488	
$Fe_{por}O_2$/vacuum (mixed)[b]	497	$Fe^{16}O-{}^{18}O$	1.0086	0.9829	0.8961	1.1451	1.0033
		$Fe^{18}O-{}^{16}O$	0.9981	0.9485	0.9160	1.1488	
$Fe_{por}O_2$/vacuum (triplet)	400	$Fe^{16}O-{}^{18}O$	1.0100	0.9829	0.8977	1.1446	1.0052
		$Fe^{18}O-{}^{16}O$	1.0005	0.9461	0.9207	1.1487	
Rh(η^2-O_2)/vacuum (singlet)	142	side-on	1.0354	0.9883	0.9959	1.0519	1.0354
$Rh_{dppe}O_2^+$/vacuum (singlet)	282	side-on	1.0178	0.9487	0.9288	1.1551	1.0178
$Rh_{dmpe}O_2^+$/vacuum (singlet)	291	side-on	1.0166	0.9525	0.9320	1.1452	1.0166
$Rh_{dmpe}O_2^+$/ClBz (singlet)	282	side-on	1.0172	0.9527	0.9321	1.1455	1.0172
$Rh_{dmpe}O_2^+$/DMF (singlet)	273	side-on	1.0184	0.9530	0.9336	1.1446	1.0184

[a] Temperature at which the ^{18}O EIE is a maximum. [b] Broken-symmetry state that mixes singlet and triplet character, ref 53.

TABLE 4: Vibrational Frequencies (cm^{-1}) Used in the Experimental and Computational Cut-Off Models

compd	mode	$^{16,16}O_2$	$^{16,18}O_2$	$^{18,16}O_2$	^{18}O $EIE_{298\ K}$[a]	^{18}O EIE_{max}[b]
$Co_{tpp}(\eta^1$-$O_2)$[c]	ν_{O-O}	1161	1129[d]	1129[d]	1.0136	1.0140 (250 K)
	ν_{M-O2}	511	511[e]	489[e]		
	δ_{M-O2}	278	262[f]	278[f]		
oxyCoHb[g]	ν_{O-O}	1136	1101[d]	1101[d]	1.0129	1.0134 (240 K)
	ν_{M-O2}	537	537[e]	516[e]		
	δ_{M-O2}	390	384[f]	390[f]		
oxyFeHb[h]	ν_{O-O}	1130	1102	1095	1.0088	1.0091 (345 K)
	ν_{M-O2}	568	557	556		
	δ_{M-O2}	425	417	410		
Co(η^1-O_2)	ν_{O-O}	1153.8	1119.4	1123.1	1.0182	1.0257 (116 K)
	ν_{M-O2}	436.3	435.7	416.8		
	δ_{M-O2}	119.7	115.7	118.1		
$Rh_{Cl}(\eta^2$-$O_2)$[i]	ν_{O-O}	890	866	866	1.0180	1.0183 (270 K)
	$\nu_{M-O2\ sym}$	581	569	569		
	$\nu_{M-O2\ asym}$	595	580	580		
Rh(η^2-O_2)	ν_{O-O}	918.9	893.2	893.2	1.0273	1.0354 (142 K)
	$\nu_{M-O2\ sym}$	479.9	469.9	469.9		
	$\nu_{M-O2\ asym}$	352.9	342.5	342.5		

[a] Calculated at 298 K. [b] Maximum EIE at the temperature noted. [c] O_2 adduct of deuterated cobalt *meso*-tetraphenylporphyrin with an axial pyridine ligand; frequencies for $Co-{}^{16,16}O_2$ and $Co-{}^{18,18}O_2$ are from ref 57. [d] $\nu_{16,18/18,16} = (\nu_{16,16} \times \nu_{18,18})^{1/2}$. [e] The stretching frequency is assumed to be equal in $Co-{}^{16}O-{}^{18}O$ and $Co-{}^{16,16}O_2$ as well as in $Co-{}^{18}O-{}^{16}O$ and $Co-{}^{18,18}O_2$. [f] The bending mode frequency is assumed to be equal in $Co-{}^{16}O-{}^{18}O$ and $Co-{}^{18,18}O_2$ as well as in $Co-{}^{18}O-{}^{16}O$ and $Co-{}^{18,18}O_2$. [g] High pH form; frequencies used for $Co-{}^{16,16}O_2$ and $Co-{}^{18,18}O_2$ are from ref 58. [h] Human oxyhemoglobin, ref 59. [i] Frequencies for $RhCl(O_2)(PPh_3)_2$(*t*-BuNC) are from ref 60.

1 as the temperature increases to infinity. The maximum normal ^{18}O EIE is observed due to the more pronounced contribution from the isotope effect on ΔS than the isotope effect on ΔH. This behavior can be understood in terms of the reduced gas-phase partition functions, which are believed to originate from similar phenomena in solution.[55,56] The ZPE terms are inverse because coordination of O_2 to a metal increases the number of oxygen isotope-sensitive vibrations and causes an increased force constant and zero-point energy level splitting in the product relative to O_2. The EXC term is also inverse for a related reason. Tightening of the force constant in the product is accompanied by an increased population of excited vibrational states to a greater extent for the heavier oxygen isotopologue than for the lighter one. The EXC decreases with increasing temperature and eventually approaches 1/MMI. At infinite temperature when all modes are equally populated, the entropic and enthalpic contributions to the ^{18}O EIE become vanishingly small.

Discussion

1. Models for Predicting Oxygen Equilibrium Isotope Effects (^{18}O EIEs). Three different approaches were used to predict oxygen equilibrium isotope effects (^{18}O EIEs) on the basis of molecular structure and compared to experimentally determined values. These approaches include (i) a full frequency model that includes all vibrations for an actual structure or a close relative, (ii) a computational three atom cutoff model that

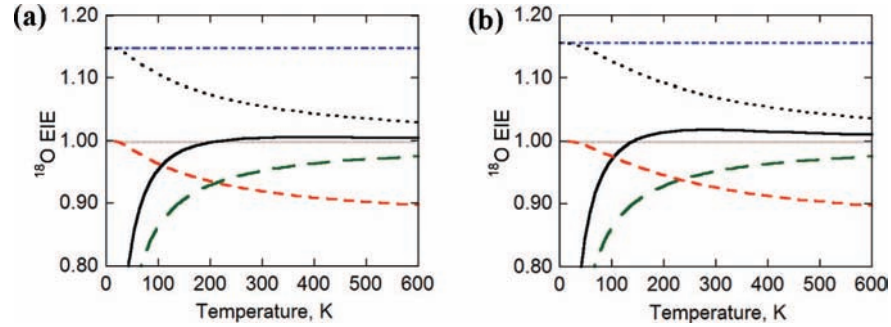

Figure 3. Temperature dependence of isotope effects and reduced gas phase partition functions for $\mathbf{Co_{sal}O_2}$ (a) and $\mathbf{Rh_{dppe}O_2^+}$ (b). The following ^{18}O EIEs (—), ZPE (— —), EXC (- - -), EXC × MMI (•••), and MMI (- • -) are calculated for full-frequency models of $\mathbf{Co_{sal}O_2}$ (left) and $\mathbf{Rh_{dppe}O_2^+}$ (right).

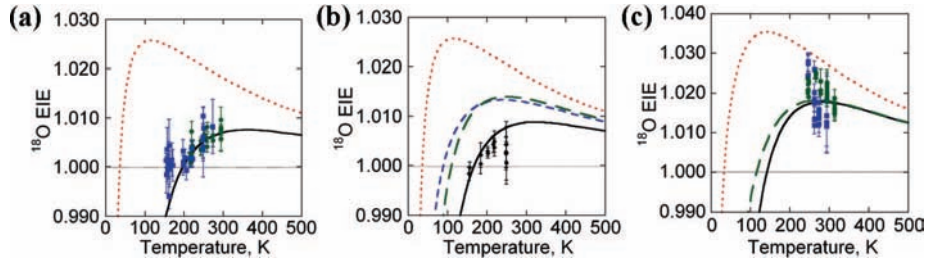

Figure 4. ^{18}O EIEs measured for (a) $\mathbf{Co_{sal}O_2}$ in MeTHF (■) and DMF (●), (b) $\mathbf{Co_{tmpp}O_2}$ in MeTHF (●), and (c) $\mathbf{Rh_{dppe}O_2^+}$ in DMF (◆) and ClBz (●). Predicted temperature profiles are shown in panels a−c for the full-frequency models (—) and computational cutoff models (•••). Experimental cutoff models are shown for **oxyCoHb** (**- - -**) and $\mathbf{Co_{tpp}(\eta^1\text{-}O_2)}$ (— —) in panel b and $\mathbf{Rh_{Cl}O_2}$ (— —) in panel c.

employs frequencies of three calculated normal modes, and (iii) an experimental cutoff model that employs frequencies of three measured vibrational modes available for related structures from the literature.

All calculations were performed by using the formalism of Bigeleisen and Goeppert−Mayer (eq 7−10).[36,37] The full-frequency model employed DFT calculations on actual or slightly modified structures with solvent corrections in some cases. The resulting ^{18}O EIEs were either normal (>1) or inverse (<1) depending on the reaction temperature. Cut-off models, analogous to those originally proposed by Wolfsberg and coworkers for reactions of "large molecules",[19] were also examined. Such models take into consideration only a subset of the most isotope-sensitive modes and, therefore, are subject to the incomplete cancelation of errors.

Though not suggested in the original studies,[19] simplified cutoff models analogous to those described by Stern and Wolfsberg have been used to interpret isotope effects on reactions of O_2.[10,16−17] These studies employed select vibrational frequencies molecules deemed relevant, which had been determined by infrared or resonance Raman spectroscopy. The η^1-superoxide structures exhibit an O−O stretch (ν_{O-O}), a symmetric metal−O stretch (ν_{M-O}), and a metal−O−O bend (δ_{M-O2}). The η^2-peroxide structures include the first two along with an asymmetric metal−O stretch ($^a\nu_{M-O}$). Frequencies of these modes were used in experimental cutoff models to predict ^{18}O EIEs for $\mathbf{Co_{sal}O_2}$, $\mathbf{Co_{tmpp}O_2}$, and $\mathbf{Rh_{dppe}O_2^+}$ as a function of temperature. Though data corresponding to actual structures were unavailable, representative examples were found and are summarized in Table 4 for β-perdeuterated cobalt *meso*-tetraphenylporphyrin with an axial pyridine molecule, $\mathbf{Co_{tpp}(\eta^1\text{-}O_2)}$,[57] a monomeric insect oxycobalt hemoglobin, **oxyCoHb**,[58] and human oxyhemoglobin, **oxyFeHb**.[59] A model based on the synthetic compound $Rh(O_2)(PPh_3)_2(t\text{-BuNC})Cl$, $\mathbf{Rh_{Cl}(\eta^2\text{-}O_2)}$, is also presented.[60]

In Table 4, the isotopic frequencies and computed isotope effects are compared to those of the computational cutoff model in which the same three vibrational frequencies were calculated for a hypothetical three-atom molecule denoted $Co(\eta^1\text{-}O_2)$ or $Rh(\eta^2\text{-}O_2)$. The comparisons indicate that the magnitude of the frequencies is underestimated in the computational cutoff model causing both the isotope effect and its temperature dependence to be inflated; this behavior is indicated by the comparison of the ^{18}O EIE at 298 K and at the temperature where the ^{18}O EIE is a maximum.

2. Computational Modeling of Measured ^{18}O EIEs. The experimental ^{18}O EIEs are compared to the results predicted by the full-frequency model, computational cutoff model, and the experimental cutoff model for $\mathbf{Co_{sal}O_2}$, $\mathbf{Co_{tmpp}O_2}$, and $\mathbf{Rh_{dppe}O_2}$ (Figure 4). As summarized in Table 5, the full frequency model consistently gives a better fit to the experimental data than either of the cutoff models, the worst of which is derived from the hypothetical three-atom structure. The ^{18}O EIEs are overestimated by the computational cutoff model because of the less inverse ZPE and EXC terms, which arise from underestimated isotope shifts of the metal−oxygen stretching and bending modes. The experimental cutoff model employs isotope shifts that are more realistic but still inadequate possibly as a result of combination vibrational modes or mode mixing.

The comparisons indicate that the full frequency models should be used whenever possible to predict ^{18}O EIEs as well as the temperature dependences. Take, for example, $\mathbf{Co_{tmpp}O_2}$, where experimental cutoff models significantly overestimate the ^{18}O EIEs at all temperatures. Further, the full-frequency calculations predict that the ^{18}O EIEs for the η^1-superoxide species should increase from low to high temperatures, the maximum value occurring above ambient. These are precisely the trends observed experimentally for $\mathbf{Co_{tmpp}O_2}$ as well as $\mathbf{Co_{sal}O_2}$.

A different situation obtains with $\mathbf{Rh_{dppe}O_2^+}$ where calculations with both experimental cutoff and full frequency models

TABLE 5: Comparison of Experimental ^{18}O Eies to Those Calculated with Full-Frequency Models

product	temp (K)	^{18}O EIE_{calc}	PCM	^{18}O EIE_{exp}	solvent
$\mathbf{Co_{sal}O_2}$	218	1.0027	DMF	1.0034 ± 0.0021	DMF
	259	1.0057		1.0041 ± 0.0011[a]	
	294	0.0069		1.0072 ± 0.0014	
$\mathbf{Co_{sal}O_2}$	161	0.9912	THF	1.0004 ± 0.0026	MeTHF
	249	1.0043		1.0056 ± 0.0025	
$\mathbf{Co_{tmpp}O_2}$	245	1.0038	none	1.0066 ± 0.0013[a]	ClBz
$\mathbf{Co_{por}O_2}$	155	0.9913	THF	0.9990 ± 0.0013[b]	MeTHF
	248	1.0039		1.0028 ± 0.0014[b]	
$\mathbf{Rh_{dppe}O_2^+}$	298	1.0177	none	1.0199 ± 0.0017[a]	DMF
$\mathbf{Rh_{dmpe}O_2^+}$	248	1.0182	DMF	1.0220 ± 0.0019[c]	DMF
	313	1.0180		1.0162 ± 0.0015[c]	
$\mathbf{Rh_{dmpe}O_2^+}$	246	1.0167	ClBz	1.0274 ± 0.0016[c]	ClBz
	295	1.0172		1.0142 ± 0.0028[c]	
$\mathbf{Fe_{por}O_2}$ (singlet)	298	0.9952	none	1.0039−1.0056[d]	water
$\mathbf{Fe_{por}O_2}$ (mixed)[e]	298	0.9998	none	1.0039−1.0056[d]	water
$\mathbf{Fe_{por}O_2}$ (triplet)	298	1.0041	none	1.0039−1.0056[d]	water

[a] Reference 22. [b] ^{18}O EIE_{exp} was determined for $\mathbf{Co_{tmpp}O_2}$; calculations with PCM were done for $\mathbf{Co_{por}O_2}$. [c] Experimental ^{18}O EIE is for $\mathbf{Rh_{dppe}O_2^+}$; calculations with PCM were done for $\mathbf{Rh_{dmpe}O_2^+}$. [d] Reference 28. [e] Broken-symmetry state that mixes singlet and triplet character, reference 53.

TABLE 6: Analysis of the Enthalpic and Entropic Contributions to the ^{18}O EIE

product	solvent	$\Delta\Delta H$ (cal/mol)	$\Delta\Delta S$ (mcal/(K × mol))	$\Delta\Delta G$ at 153 K (cal/mol)	$\Delta\Delta G$ at 298 K (cal/mol)
$\mathbf{Co_{sal}O_2}$	DMF	8.0 ± 1.2	43 ± 5	1.4 ± 1.4 (0.9954)[b]	-4.8 ± 1.9 (1.0081)[a]
$\mathbf{Co_{sal}O_2}$	MeTHF	4.4 ± 0.9	27 ± 4	0.3 ± 1.1 (0.9990)[a]	-3.6 ± 1.5 (1.0061)[a]
$\mathbf{Co_{tmpp}O_2}$	MeTHF	4.4 ± 1.2	27 ± 6	0.3 ± 1.5 (0.9990)[a]	-3.6 ± 2.2 (1.0061)[a]

[a] $\Delta\Delta H$ and $\Delta\Delta S$ defined as the light minus heavy isotopologues with errors of $\pm 2\sigma$. [b] The corresponding ^{18}O EIE is given in parentheses.

imply reasonable agreement to the empirical results and only the computational cutoff model is inadequate. Though the level of agreement between the calculated and measured isotope effect is excellent at ambient temperature, it deteriorates at lower temperatures. The experimental ^{18}O EIEs become larger while the models predict a plateau region. Presently, these results are attributed to a systematic experimental error arising from incomplete sample equilibration. The experiments above 245 K suggest that the ^{18}O EIE decreases with increasing temperature, opposite to the behavior projected for the η^1-superoxide structures.

Oxygen transporting heme proteins, hemoglobin and myoglobin, bind O_2 in an end-on manner similar to that observed in $\mathbf{Co_{sal}O_2}$ and $\mathbf{Co_{tmpp}O_2}$. The ^{18}O EIEs determined for these proteins range from 1.0039 to 1.0056 at physiological pH and ambient temperature.[28] We attempted to model these values using experimental cutoff (Table 4) and theoretical full-frequency models (Table 5). The experimental cutoff model predicts an ^{18}O EIE of >1.0088, significantly larger than the measured effects. The full-frequency models include gas-phase geometry optimizations of the singlet, broken-symmetry, and triplet states of the η^1-superoxide species, $\mathbf{Fe_{por}O_2}$. These calculations show that the ^{18}O EIE predicted for the triplet $\mathbf{Fe_{por}O_2}$ (1.0041) matches the experimental value better than the singlet and broken-symmetry states for which inverse ^{18}O EIEs (0.9952 and 0.9998) are predicted (Table 5). Oxyhemoglobin exhibits a temperature-dependent magnetic moment due to antiferromagnetic coupling,[61] therefore, the observation that the full frequency calculations give mixed results, with the triplet state exactly reproducing the experimental result, is not surprising. The determination of spin-state energies for systems with multiple unpaired electrons remains a computational challenge.[29,62]

3. Are Experimental Cutoff Models Satisfactory? The question arises of how useful experimental cutoff models are in interpreting ^{18}O EIEs for O_2 activation reactions. On the basis of the results in Figure 4, it appears that the cutoff model is unable to reproduce experimental trends for η^1-structures but performs reasonably for η^2-structures. In view of the importance of low-frequency bending modes in the former, the inadequacy of the cutoff model likely reflects the end-on geometry rather than the extent of O−O reduction.

The most obvious problem with the cutoff model is the inherent deviation from the Redlich−Teller Product Rule, which requires all vibrational frequencies to be considered in the calculation of MMI. In applications where some fraction of the isotope shift is neglected, MMI_{VP} (eq 10) can be up to three times less than MMI_{rot} (eq 11), even though the terms should be equivalent. For this reason, the ZPE and EXC contributions are significantly less inverse than expected from the full frequency calculations. The reduced partition functions translate into inflated ^{18}O EIEs with consistently smaller differences between the η^1-superoxide and η^2-peroxide structures than indicated by experimental studies.[22]

In spite of these deficiencies, the trends in ^{18}O EIEs with temperature are roughly similar for the experimental cutoff and full frequency models described in this study; yet only the full frequency is able to accurately reproduce the experimental results. We attribute the similar predictions to compensating entropic and enthalpic influences as well as the cancelation of errors (Table 6). In general, the full frequency model is more reliable and gives a more realistic impression of the physical origins of the ^{18}O EIEs discussed below.

4. Enthalpic and Entropic Contributions. The ^{18}O EIE is theoretically equal to the equilibrium constant for an isotope exchange reaction. Enthalpic and entropic contributions can, therefore, be estimated through analysis using the van't Hoff equation. Plotting the data for $\mathbf{Co_{sal}O_2}$ and $\mathbf{Co_{tmpp}O_2}$ as ln(^{18}O EIE) versus $1/T$ gives a straight line from 153 to 298 K with a slope of $-\Delta\Delta H/R$ and y-intercept of $\Delta\Delta S/R$ (Figure 5). Yet deviations are expected over large ranges in accord with Figure 3. Due to experimental limitations, together with the uncertainty

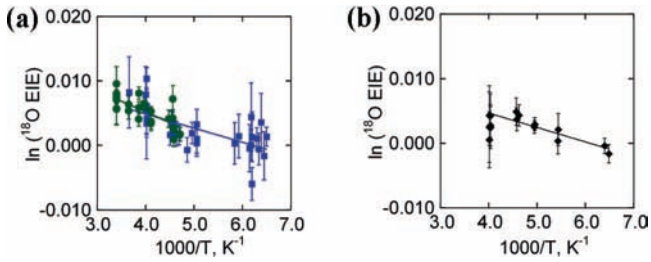

Figure 5. van't Hoff analysis: (a) $\mathbf{Co_{sal}O_2}$ in MeTHF (■) and DMF (●) and (b) $\mathbf{Co_{tmpp}O_2}$ in MeTHF (◆). The data are weighted by $\pm 2\sigma$ error bars.

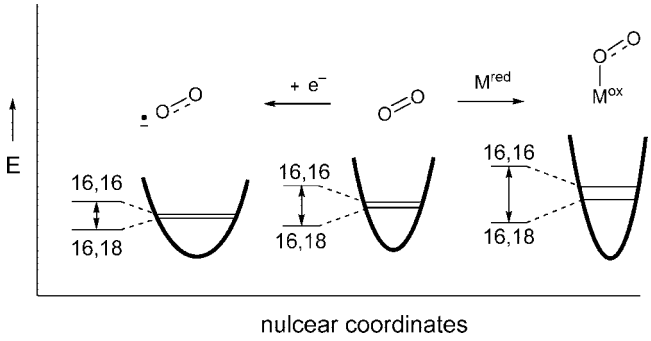

Figure 6. Zero point energy changes upon outer-sphere or inner-sphere reduction of O_2.

in the ^{18}O EIE, $\mathbf{Rh_{dppe}O_2^+}$ could not be included in the analysis which follows.

The van't Hoff plots of ln(^{18}O EIE) versus $1/T$ for $\mathbf{Co_{sal}O_2}$ and $\mathbf{Co_{tmpp}O_2}$ exhibit negative slopes in MeTHF and DMF. Since by definition $\Delta\Delta H = {}^{16,16}\Delta H - {}^{16,18}\Delta H$, an inverse enthalpic isotope effect is observed ranging from +4.4 to +8.0 cal mol^{-1}, well outside the error limits. The inverse effect reflects the tighter binding of the heavier isotopologue to the metal than the lighter one. The three independent measurements, thus, provide compelling support for the inverse ZPE depicted in Figure 6. Though this behavior is predicted by the full frequency model it is not adequately reproduced by the cutoff models because of the insufficient number of vibrational frequencies considered.

Furthermore, we emphasize that the inverse nature of the ZPE is opposite to that expected on the basis of the changing O−O force constant. This is perhaps the most surprising result since in earlier works, the change in this force constant was assumed to be the primary determinant of the ^{18}O EIE.[9c,28] The van't Hoff analysis provides evidence to the contrary and reflects the origin of the isotope effect in terms of the bond strengths within the oxygenated product relative to O_2. In reactions where O_2 coordinates to a reduced metal center, an inverse enthalpic effect is offset by a dominant normal entropic effect causing the overall ^{18}O EIE to be normal. This is expected to be the origin of heavy atom isotope effects on small molecule activation in general where the extent of electron transfer strengthens bonds to the metal at the expense of losing translation and rotational degrees of freedom.

Conclusions

This is the first rigorous examination of the physical origins of the equilibrium isotope effects on the reversible coordination of O_2 to transition metal centers. Experiments reveal that solvent polarity has no discernible influence on the magnitude of the oxygen isotope effects but that trends with temperature can be resolved over sufficiently large ranges, i.e. >50 deg K. Depending on the contributions of low-frequency isotopic modes, the oxygen isotope effect may increase or decrease as the temperature is raised. In this study, matching experimental and computational results have been obtained for the temperature dependence of the equilibrium isotope effects, consistent with an inverse enthalpic isotope effect and normal entropic isotope effect described below.

The competitive binding of ^{16}O−^{16}O versus ^{16}O−^{18}O is influenced by compensating enthalpic and entropic factors. For two structurally similar superoxide compounds, van't Hoff analysis indicates an inverse isotope effect on the reaction enthalpy but a normal isotope effect overall. This behavior is consistent with the predominance of a normal entropic isotope effect over the temperature range investigated. Importantly, the inverse enthalpic effect and dominant entropic effect are counter to the trends expected for an isolated change in O−O force constant as O_2 is reduced to superoxide and peroxide species.

Three different models for predicting the temperature dependence of the oxygen equilibrium isotope effects were evaluated. A full frequency model, which includes all vibrational frequencies derived from density functional theory calculations on actual structures or close relatives, is found to be superior to cutoff models. Two cutoff models were examined, one which employed a hypothetic three-atom structure and one which used experimental vibrational frequencies associated with the most isotope-sensitive stretching and bending modes. Only the full frequency model was able to accurately and reliably reproduce the experimental differences in the magnitudes of the isotope effects as well as the temperature variations for end-on superoxide structures.

Though there are still limitations in the ability to predict heavy atom isotope effects with use of vibrational frequencies from density functional theory calculations, this work represents a significant advance in modeling the temperature-dependent and -independent contributions. To reiterate, the analyses demonstrate that both enthalpic and entropic components are important when small molecules coordinate to reduced transition metal centers. The normal isotope effect on the reaction entropy is found to dominate in reversible O_2 binding reactions over the experimental temperature range. Future efforts will be directed toward understanding whether the same holds true for the oxygen kinetic isotope effects which characterize the related O_2 association reactions.

Appendix

The ^{18}O EIE is represented in this work as a weighted geometric mean[63a] according to eq A-1, where the individual EIEs represent the M−^{18}O−^{16}O and M−^{16}O−^{18}O coordination modes relative to M−^{16}O−^{16}O. The weighting term, α, represents the fraction of metal−O_2 adduct with ^{16}O−^{18}O coordinated via the heavy isotope (^{18}O). The mathematical definition, $\alpha = [M-{}^{18}O-{}^{16}O]/\{[M-{}^{18}O-{}^{16}O] + [M-{}^{16}O-{}^{18}O]\}$, requires α to fall between 0 and 1. The expression for the weighted geometric mean (eq A-1) is derived below and α is recast in terms of the individual isotope effects calculated from the Bigeleisen/Goeppert−Mayer formalism.

$$^{18}\text{O EIE}_{\text{WGM}} = (^{18,16}\text{O EIE})^{\alpha} \times (^{16,18}\text{O EIE})^{(1-\alpha)} \quad \text{(A-1)}$$

When ^{16}O−^{18}O coordinates end-on to a metal, the following equilibrium occurs:

$$M + {}^{16}O-{}^{18}O \rightleftarrows \alpha M-{}^{18}O-{}^{16}O + (1-\alpha)M-{}^{16}O-{}^{18}O \quad \text{(A-2)}$$

The equilibrium constant, ${}^{(16,18)}K_{eq}$, corresponding to the competition of the mixed isotopologue of oxygen for the two different bonding modes is given by:

$${}^{(16,18)}K_{eq} = \frac{[M^{18}O^{16}O]^{\alpha} \times [M^{16}O^{18}O]^{(1-\alpha)}}{[M][{}^{16,18}O_2]} \quad \text{(A-3)}$$

Since $[M] = [M]^{\alpha} \times [M]^{(1-\alpha)}$ and $[O_2] = [O_2]^{\alpha} \times [O_2]^{(1-\alpha)}$, eq A-3 can be rewritten as:

$${}^{(16,18)}K_{eq} = \left(\frac{[M^{18}O^{16}O]}{[M][{}^{16,18}O_2]}\right)^{\alpha} \times \left(\frac{[M^{16}O^{18}O]}{[M][{}^{16,18}O_2]}\right)^{(1-\alpha)} \quad \text{(A-4)}$$

Inserting the equilibrium constants, ${}^{18,16}K_{eq}$ and ${}^{16,18}K_{eq}$, defined by the terms in parentheses gives:

$${}^{(16,18)}K_{eq} = {}^{18,16}K_{eq}{}^{\alpha} \times {}^{16,18}K_{eq}{}^{(\alpha-1)} \quad \text{(A-5)}$$

Equating ${}^{(16,18)}K_{eq}$ to ${}^{16,18}K_{eq}$ in eq 1 and treating the light isotopologue analogously, by inserting ${}^{16,16}K_{eq} = {}^{16,16}K_{eq}{}^{\alpha} \times {}^{16,16}K_{eq}{}^{(1-\alpha)}$, results in:

$${}^{18}O\ EIE = \frac{{}^{16,16}K_{eq}{}^{\alpha} \times {}^{16,16}K_{eq}{}^{(1-\alpha)}}{{}^{18,16}K_{eq}{}^{\alpha} \times {}^{16,18}K_{eq}{}^{(1-\alpha)}} \quad \text{(A-6)}$$

Regrouping this expression gives the definition of the ${}^{18}O$ EIE as a weighted geometric mean (A-1):

$${}^{18}O\ EIE = \left(\frac{{}^{16,16}K_{eq}}{{}^{18,16}K_{eq}}\right)^{\alpha} \times \left(\frac{{}^{16,16}K_{eq}}{{}^{16,18}K_{eq}}\right)^{(1-\alpha)} \quad \text{(A-7)}$$

The α is defined as the fraction of metal$-O_2$ adduct with ${}^{16}O-{}^{18}O$ coordinated via the heavy oxygen isotope. The parameter can equivalently be expressed in terms of individual equilibrium constants:

$$\alpha = {}^{18,16}K_{eq}/({}^{18,16}K_{eq} + {}^{16,18}K_{eq}) \quad \text{(A-8)}$$

Redefining the individual equilibria in terms of the overall ${}^{18}O$ EIE gives:

$$\alpha = \frac{1}{{}^{18,16}O\ EIE} \times {}^{16,16}K_{eq} / \left(\frac{1}{{}^{18,16}O\ EIE} \times {}^{16,16}K_{eq} + \frac{1}{{}^{16,18}O\ EIE} \times {}^{16,16}K_{eq}\right) \quad \text{(A-9)}$$

After cancelation of ${}^{16,16}K_{eq}$ and rearrangement, the following simplified expression is obtained:

$$\alpha = \frac{1}{1 + \frac{{}^{18,16}O\ EIE}{{}^{16,18}O\ EIE}} \quad \text{(A-10)}$$

Acknowledgment. We gratefully acknowledge support from the National Science Foundation CAREER award (CHE-0449900), a Research Corporation Cottrell Scholar Award, an Alfred P. Sloan Foundation fellowship, and a Camille Dreyfus Teacher Scholar Award to J.P.R.

References and Notes

(1) (a) Urey, H. C.; Greiff, L. J. *J. Am. Chem. Soc.* **1935**, *57*, 321. (b) Bigeleisen, J. *J. Phys. Chem.* **1952**, *56*, 823.

(2) (a) Dole, M.; Lane, G. A.; Rudd, D. P.; Zaukelies, D. A. *Geochim. Cosmochim. Acta* **1954**, *6*, 65. (b) Feldman, D. E.; Yost, H. T., Jr.; Benson, B. E. *Science* **1959**, *129*, 146. (c) DeNiro, M. J.; Epstein, S. *Science* **1979**, *204*, 51.

(3) (a) Cook, P. F., Ed. *Enzyme Mechanisms from Isotope Effects*; CRC Press:Boca Raton, FL, 1991. (b) Melander, L. C.; Saunders, W. H. *Reaction Rates of Isotopic Molecules*; Wiley: New York, 1980.

(4) (a) Cleland, W. W. *Methods Enzymol.* **1995**, *249*, 341. (b) Cleland, W. W. *Arch. Biochem. Biophys.* **2005**, *433*, 2.

(5) Thiemans, M. *Annu. Rev. Earth Planet. Sci.* **2006**, *34*, 217.

(6) Hofstetter, T. B.; Neumann, A.; Arnold, W. A.; Hartenbach, A. E.; Bolotin, J.; Cramer, C. J.; Schwarzenbach, R. P. *Environ. Sci. Technol.* **2008**, *42*, 1997.

(7) Gao, Y. Q.; Marcus, R. A. *Science* **2001**, *293*, 259.

(8) Epstein, S.; Zeiri, L. *Proc. Natl. Acad. Sci. U.S.A.* **1988**, *85*, 1727.

(9) (a) Roth, J. P. *Acc. Chem. Res.* **2008**,in press. (b) Roth, J. P. *Curr. Opin. Chem. Biol.* **2007**, *11*, 142. (c) Roth, J. P.; Klinman, J. P. In *Isotope Effects in Chemistry and Biology*; Kohen, A., Limbach, H.-H., Eds.; CRC Press: Boca Raton, FL, 2006; p 645.

(10) Smirnov, V. V.; Roth, J. P. *J. Am. Chem. Soc.* **2006**, *128*, 3683.

(11) Smirnov, V. V.; Roth, J. P. *J. Am. Chem. Soc.* **2006**, *128*, 16424.

(12) Roth, J. P.; Cramer, C. J. *J. Am. Chem. Soc.* **2008**, *130*, 7802.

(13) (a) Prabhakar, R.; Siegbahn, P. E. M.; Minaev, B. F.; Agren, H. *J. Phys. Chem. B* **2004**, *108*, 13882. (b) Lundberg, M.; Morokuma, K. *J. Phys. Chem. B* **2007**, *111*, 9380. (c) Gherman, B. F.; Baik, M.-H.; Lippard, S. J.; Friesner, R. A. *J. Am. Chem. Soc.* **2004**, *126*, 2978. (d) Metz, M.; Solomon, E. I. *J. Am. Chem. Soc.* **2001**, *123*, 4938. (e) Brunold, T. C.; Solomon, E. I. *J. Am. Chem. Soc.* **1999**, *121*, 8288.

(14) (a) Durrant, M. C. *Biochemistry* **2002**, *41*, 13934. (b) Studt, F.; Tuczek, F. *J. Comput. Chem.* **2006**, *27*, 1278.

(15) (a) Popp, B. V.; Wendlandt, J. E.; Landis, C. R.; Stahl, S. S. *Angew. Chem., Int. Ed.* **2007**, *46*, 601. (b) Studt, F.; Lamarche, V. M. E.; Clentsmith, G. K. B.; Cloke, F.; Geoffrey, N.; Tuczek, F. *Dalton Trans.* **2005**, 1052. (c) Aboelella, N. W.; Kryatov, S. V.; Gherman, B. F.; Brennessel, W. W.; Young, V. G., Jr.; Sarangi, R.; Rybak-Akimova, E. V.; Hodgson, K. O.; Hedman, B.; Solomon, E. I.; Cramer, C. J.; Tolman, W. B. *J. Am. Chem. Soc.* **2004**, *126*, 16896. (d) Schenk, G.; Pau, M.Y. M.; Solomon, E. I. *J. Am. Chem. Soc.* **2004**, *126*, 505. (e) Laplaza, C. E.; Johnson, M. J. A.; Peters, J.; Odom, A. L.; Kim, E.; Cummins, C. C.; George, G. N.; Pickering, I. J. *J. Am. Chem. Soc.* **1996**, *118*, 8623.

(16) (a) Burger, R. M.; Tian, G.; Drlica, K. *J. Am. Chem. Soc.* **1995**, *117*, 1167. (b) Mirica, L. M.; McCusker, K. P.; Munos, J. W.; Liu, H.-w.; Klinman, J. P. *J. Am. Chem. Soc.* **2008**, *130*, 8122.

(17) Lanci, M. P.; Brinkley, D. W.; Stone, K. L.; Smirnov, V. V.; Roth, J. P. *Angew. Chem., Int. Ed.* **2005**, *44*, 7273.

(18) A related example for H_2 addition is described in: Abu-Hasanayn, F.; Goldman, A. S.; Krogh-Jespersen, K. *J. Phys. Chem.* **1993**, *97*, 5890.

(19) Stern, M. J.; Wolfsberg, M. *J. Phys. Chem.* **1966**, *45*, 4105.

(20) Armarego, W.; Chai, C. *Purification of Laboratory Chemicals; Butterworth-Heinemann*: Amsterdam, The Netherlands, 2003.

(21) (a) Collman, J.; Sears, C.; Kubota, M. *Inorg. Synth.* **1968**, *11*, 101. (b) DeStefano, N. J.; Burmeister, J. L. *Inorg. Chem.* **1971**, *10*, 998. (c) Miller, J. S.; Caulton, K. G. *J. Am. Chem. Soc.* **1975**, *97*, 1067. (d) Drago, R.; Cannady, P.; Leslie, K. *J. Am. Chem. Soc.* **1980**, *102*, 6014.

(22) Lanci, M. P.; Roth, J. P. *J. Am. Chem. Soc.* **2006**, *128*, 16006.

(23) Rybak-Akimova, E. V.; Otto, W.; Deardorf, P.; Roesner, R.; Busch, D. H. *Inorg. Chem.* **1997**, *36*, 2746.

(24) (a) Zou, S.; Baskin, J. S.; Zewail, A. H. *Proc. Natl. Acad. Sci. U.S.A.* **2002**, *99*, 9625. (b) Walker, F. A. *J. Am. Chem. Soc.* **1973**, *95*, 1150. (c) Walker, F. A. *J. Am. Chem. Soc.* **1973**, *95*, 1154.

(25) Geoffroy, G. L.; Wrighton, M. S.; Hammond, G. S.; Gray, H. B. *J. Am. Chem. Soc.* **1974**, *96*, 3105.

(26) Laidler, K. J. *Chemical Kinetics*, 3rd ed.; Harper Collins: New York, 1987; p 30.

(27) Barshop, B. A.; Wrenn, R. F.; Frieden, C. *Anal. Biochem.* **1983**, *130*, 134.

(28) Tian, G.; Klinman, J. P. *J. Am. Chem. Soc.* **1993**, *115*, 8891.

(29) Lanci, M. P.; Smirnov, V. V.; Cramer, C. J.; Gauchenova, E. V.; Sundermeyer, J.; Roth, J. P. *J. Am. Chem. Soc.* **2007**, *129*, 14697.

(30) (a) Perdew, J. P.; Wang, Y. *Phys. Rev. B* **1986**, *33*, 8800. (b) Perdew, J. P. In *Electronic Structure of Solids '91*; Ziesche, P., Eschrig, H., Eds.; Akademie Verlag: Berlin, Germany, 1991; p 11. (c) Adamo, C.; Barone, V. *J. Chem. Phys.* **1998**, *108*, 664.

(31) Frisch, M. J.; et al. *Gaussian 03W*, Revision C.02; Gaussian, Inc.: Pittsburgh, PA, 2003.

(32) Stevens, W. J.; Krauss, M.; Basch, H.; Jasien, P. G. *Can. J. Chem.* **1992**, *70*, 612.

(33) Hehre, W. J.; Radom, L.; Schleyer, P. v. R.; Pople, J. A. *Ab Initio Molecular Orbital Theory*; Wiley: New York, 1986.

(34) (a) Cramer, C. J.; Tolman, W. B.; Theopold, K. H.; Rheingold, A. L. *Proc. Natl. Acad. Sci. U.S.A.* **2003**, *100*, 3635. (b) Kinsinger, C. R.; Gherman, B. F.; Gagliardi, L.; Cramer, C. J. *J. Biol. Inorg. Chem.* **2005**, *10*, 778.

(35) (a) Kolmodin, K.; Luzhkov, V. B.; Aqvist, J. *J. Am. Chem. Soc.* **2002**, *124*, 10130. (b) Headley, G. W.; O'Leary, M. H. *J. Am. Chem. Soc.* **1990**, *112*, 1894.

(36) Bigeleisen, J.; Goeppert-Mayer, M. *J. Chem. Phys.* **1947**, *15*, 261.

(37) Bigeleisen, J.; Wolfsberg, M. *Adv. Chem. Phys.* **1958**, *1*, 15.

(38) Redlich, O. *Z. Phys. Chem.* **1935**, *B28*, 371.

(39) (a) Blair, M. M. *Elementary Statistics with General Applications*; H. Holt and Company: New York, 1952. (b) Zwillinger, D. *CRC Standard Mathematical Tables and Formulae*, 31st ed.; Chapman & Hall/CRC Press: Boca Raton, FL, 2003.

(40) Purdy, M. M.; Koo, L. S.; Ortiz de Montellano, P. R.; Klinman, J. P. *Biochemistry* **2006**, *45*, 15793.

(41) (a) Dong, Y.; Menage, S.; Brennan, B. A.; Elgren, T. E.; Jang, H. G.; Pearce, L. L.; Que, L. *J. Am. Chem. Soc.* **1993**, *115*, 1851. (b) Imai, H.; Kyuno, E. *Inorg. Chim. Acta* **1988**, *153*, 183.

(42) Janak, K. E.; Parkin, G. *J. Am. Chem. Soc.* **2003**, *125*, 13219.

(43) Wolfsberg, M. In *Isotope Effects in Chemistry and Biology*; Kohen, A., Limbach, H.-H., Eds.; CRC Press: Boca Raton, FL, 2006; p 89.

(44) Cini, R.; Orioli, P. *J. Chem. Soc., Dalton Trans.* **1983**, 2563.

(45) Petsko, G. A.; Rose, D.; Tsernoglou, D.; Ikeda-Saito, M.; Yonetani, T. In *Frontiers of Biological Energetics*; Dutton, P. L., Scarpa, A., Leigh, J. S., Eds.; Academic Press: New YorK, 1978; p 1011.

(46) James, B. R.; Mahajan, D. *Can. J. Chem.* **1980**, *58*, 996.

(47) Hill, H. A. O.; Tew, D. G. In *Comprehensive Coordination Chemistry: Synthesis, Reaction, Properties, and Applications of Coordination Compounds*; Wilkinson, G., Gillard, R. D., McCleverty, J. A., Eds.; Pergamon Press: Oxford, England, 1987; Vol. 2, p 315.

(48) Chase, M. W., Jr.; Curnutt, J. L.; Downey, J. R., Jr.; McDonald, R. A.; Syverud, A. N.; Valenzuela, E. A. *J. Phys. Chem. Ref. Data* **1982**, *11*, 695.

(49) Krupenie, P. H. *J. Phys. Chem. Ref. Data* **1972**, *1*, 423.

(50) Nakamoto, K.; Paeng, I. R.; Kuroi, T.; Isobe, T.; Oshio, H. *J. Mol. Struct.* **1988**, *189*, 293.

(51) Bajdor, K.; Nakamoto, K.; Kanatomi, H.; Murase, I. *Inorg. Chim. Acta* **1984**, *82*, 207.

(52) Gubelmann, M. H.; Williams, A. F. *Struct. Bonding (Berlin)* **1983**, *55*, 1.

(53) Cramer, C. J. *Essentials of Computational Chemistry*, 2nd ed.; Wiley: Chichester, England, 2004.

(54) For temperature dependence of ^{18}O EIEs on O_2 binding to copper complexes see ref 29.

(55) (a) Bigeleisen, J. *J. Chem. Phys.* **1961**, *34*, 1485. (b) Herzfeld, K. F.; Teller, E. *Phys. Rev.* **1938**, *54*, 912.

(56) Slaughter, L. M.; Wolczanski, P. T.; Klinckman, T. R.; Cundari, T. R. *J. Am. Chem. Soc.* **2000**, *122*, 7953.

(57) Weselucha-Birczynska, A.; Nakamoto, K.; Proniewicz, L. M. *J. Mol. Struct.* **1992**, *275*, 95.

(58) Thompson, H. M.; Yu, N.-T.; Gersonde, K. *Biophys. J.* **1987**, *51*, 289.

(59) Hirota, S.; Ogura, T.; Appleman, E. H.; Shinzawa-Itoh, K.; Yoshikawa, S.; Kitagawa, T. *J. Am. Chem. Soc.* **1994**, *116*, 10564.

(60) Nakamura, A.; Tatsuno, Y.; Yamamoto, M.; Otsuka, S. *J. Am. Chem. Soc.* **1971**, *93*, 6052.

(61) (a) Philo, J. S.; Dreyer, U.; Schuster, T. M. *Biochemistry* **1984**, *23*, 865. (b) Pauling, L. *Proc. Natl. Acad. Sci. U.S.A.* **1977**, *74*, 2612.

(62) de la Lande, A.; Moliner, V.; Parisel, O. *J. Chem. Phys.* **2007**, *126*, 035102/1.

(63) (a) Blair, M. M. *Elementary Statistics with General Applications*; H. Holt and Company: New York, NY, 1952. (b) Zwillinger, D. *CRC Standard Mathematical Tables and Formulae*, 31st ed.; Chapman & Hall/CRC Press: Boca Raton, FL, 2003.

JP807796C